Nature Geoscience
September 2018, Volume 11 Issue 9 Pages 665-671
https://doi.org/10.1038/s41561-018-0190-9
https://archimer.ifremer.fr/doc/00638/74977/

Microbial life and biogeochemical cycling on land 3,220 million years ago

Homann Martin [1, *], Sansjofre Pierre [1], Van Zuilen Mark [2], Heubeck Christoph [3], Gong Jian [2], Killingsworth Bryan [1], Foster Ian S. [1], Airo Alessandro [4], Van Kranendonk Martin J. [5, 6], Ader Magali [3], Lalonde Stefan [1]

[1] European Inst Marine Studies, CNRS, UMR6538, Lab Geosci Ocean, Technopole Brest Iroise, Plouzane, France.
[2] Inst Phys Globe Paris, CNRS, UMR7154, Paris, France.
[3] Friedrich Schiller Univ, Dept Geosci, Jena, Germany.
[4] Tech Univ Berlin, Ctr Astron & Astrophys, Berlin, Germany.
[5] Univ New South Wales, Australian Ctr Astrobiol, Sydney, NSW, Australia.
[6] Univ New South Wales, Sch Biol Earth & Environm Sci, Sydney, NSW, Australia.

* Corresponding author : Martin Homann, email address : martin.homann@univ-brest.fr

Abstract :

The colonization of emergent continental landmass by microbial life was an evolutionary step of paramount importance in Earth history. Here we report direct fossil evidence for life on land 3,220 million years ago (Ma) in the form of terrestrial microbial mats draping fluvial conglomerates and gravelly sandstones of the Moodies Group, South Africa. Combined field, petrographic, carbon isotope and Raman spectroscopic analyses confirm the synsedimentary origin and biogenicity of these unique fossil mats as well as their fluvial habitat. The carbon isotope compositions of organic matter (delta C-13(org)) from these mats define a narrow range centred on -21 parts per thousand, in contrast to fossil mats of marine origin from nearby tidal deposits that show delta C-13(org) values as low as -34 parts per thousand. Bulk nitrogen isotope compositions (2 < delta N-15 < 5 parts per thousand) are also significantly different from their marine counterparts (0 < delta N-15 < 3 parts per thousand), which we interpret as reflecting denitrification in the terrestrial habitat, possibly of an atmospheric source of nitrate. Our results support the antiquity of a thriving terrestrial biosphere during the Palaeoarchaean and suggest that a complex and microbially driven redox landscape existed during the deposition of the Moodies Group, with distinct biogeochemical cycling occurring on land by 3,220 Ma.

While there is abundant evidence that microbial life thrived in the oceans as far back as there is a sedimentary record[1–5], significantly less is known about microbial colonization of the land surface. Before 3,000 Myr ago, much of the Earth may have been submerged[6], and accordingly, direct fossil evidence for terrestrial[7] life prior to the Mesoarchean is extremely rare[8,9]. It is also

inferential, largely derived from the study of paleosols as old as 3,200 Myr[10–14]. A suite of suggestive biosignatures in hot spring deposits indicate that life may have already been occupying terrestrial niches by 3,480 Myr[15]. Here we present the discovery of a new locality in the Paleoarchean Moodies Group, Barberton Greenstone Belt (BGB), South Africa, where exceptionally-preserved microbial mats are exposed in sediments of an ancient fluvial system. These terrestrial fossils represent a significant expansion of the known diversity of microbial life in the Moodies Group, which until now has been restricted solely to marine settings[16–20].

The Moodies Group is the uppermost of the three stratigraphic units constituting the Barberton Greenstone Belt (Supplementary Fig. 1) and represents the world's oldest well-preserved alluvial to shallow marine deposit[21,22]. It consists of a thick (up to 3.5 km) succession of alluvial to shallow-marine quartz-rich sandstones with subordinate conglomerates, mudstones, thin tuffs, banded iron formations, and a single basaltic lava[22]. The age of the Moodies Group is tightly constrained by several dacitic tuffs and rare felsic dikes radiating from the Kaap Valley tonalite that crosscut the Moodies Group along the northern margin of the BGB. U-Pb dating of single-zircons from these units indicate that deposition began about 3,223 ± 1 Myr and had ended by about 3,219 ± 9 Myr[23,24]. The southwestward-plunging Dycedale Syncline, approx. 2 km east of Barberton, hosts a steeply dipping >350 m thick succession of Moodies Group conglomerates and cross-bedded sandstones. A large variety of sedimentary structures indicates that this succession records a transition from alluvial-fluvial (terrestrial) to tide-influenced marine sedimentation[21,22] (Supplementary Fig. 2).

Terrestrial microbial mats in fluvial sandstones

Our study is focused on fossilized microbial mats discovered in this unique terrestrial-to-marine transition in the Dycedale Syncline. The base of the section begins with a ~75-m-thick sedimentary unit including a ~40 m thick, polymict, mostly clast-supported conglomerate in

64 the central part (unit B of ref. 22; Supplementary Fig. 2). The poor sorting and angularity of
65 clasts, poorly developed internal fabrics, clast imbrication, thin intercalated sandstone beds with
66 upper-plane bed horizontal lamination, and the immature composition of this conglomerate
67 indicate a proximal sediment source associated with episodic, short-lived, high-energy
68 unidirectional transport. These fabrics and associations are typical for sheet flow-dominated
69 alluvial fans and/or proximal braided streams with highly variable discharge. The conglomerate
70 is under- and overlain by 10- and 25-m-thick (respectively) gravelly sandstones with
71 carbonaceous laminations and minor interbedded conglomerate beds. These lens- or wedge-
72 shaped beds are 0.2 to 2 m thick, commonly vertically stacked, and show minor channel incision
73 from erosional downcutting, characteristic of fluvial deposition and transport (Fig. 1a). Pebble-
74 to boulder-sized clasts (up to ~40 x 40 cm) are subrounded, poorly-sorted, and embedded in a
75 quartz-rich coarse-sandy matrix (Fig. 1b). The transition to overlying gravelly, medium- to
76 coarse-grained quartzofeldspathic sandstones is gradational. These horizontal to low-angle
77 planar cross-bedded sandstones are locally interbedded with discontinuous mudstones with
78 desiccation cracks, indicating periods of subaerial exposure (Supplementary Fig. 3). Overlying
79 strata gradually deepen upward through deltaic, and medium-energy tidal, into subtidal
80 siliciclastic deposits. The position of the conglomerate-bearing deposits at the base of this
81 transgressive, fining- and deepening-upward sequence, and the absence of any sedimentary
82 structure indicative of tidal or marine conditions, further suggests that the gravelly sandstones
83 and conglomerates represent a terrestrial depositional environment, likely a fluvial coastal
84 braidplain that was updip of an estuary[22].
85
86 The wavy and crinkly carbonaceous laminations within these gravely sandstones and on top of
87 the conglomerate beds show a variety of features consistent with a biogenic origin. They are
88 densely spaced at the mm-scale, and both onlap and drape protruding clasts (Fig.1c-d). Laminae
89 are bent upwards and plastically deformed by 10- to 50-cm-high subvertical fluid-escape

structures, indicating their cohesive water-impermeable nature and synsedimentary origin (Fig. 1e, Supplementary Fig. 4). A high strength and cohesiveness of the laminae is further supported by their association with coarse-grained sandstone and conglomerate beds that were repeatedly emplaced on top of the laminae without severely damaging or eroding them (Fig. 2a). However, petrographic analysis also reveals that during periods of increased current velocity, and therefore higher shear stress, laminae were partially eroded, ripped up and reworked as fragments of up to several cm in length (Fig. 2a and 2c-f). In thin section, the 0.5 - 4 mm thick laminae are composed of a dense meshwork of interwoven filament-like microstructures that drape horizontally laminated and rippled sandstones, onlap individual clasts, and envelop "floating" detrital grains of fine-grained sand whose long axes are preferentially aligned parallel to bedding (Fig. 2a-b). Individual carbonaceous filamentous structures are 1 - 3 µm in diameter and may exceed 100 µm in length, commonly bundled and twisted around each other (Fig. 2c; Supplementary Fig. 5), consistent with, but not exclusive to, modern filamentous microorganisms forming biofilms. The excellent preservation of these features is thought to be due to a combination of very early silicification, low tectonic strain, and the low temperature of post-depositional hydrothermal overprinting (<150°C) in the interior part of the Barberton Greenstone Belt[19,25]. Raman microspectroscopy demonstrates that the carbonaceous laminae of both the terrestrial and marine mats[19] are composed of organic carbon that has experienced similar peak temperatures of ~365°C (see Methods), consistent with the metamorphic grade of lower greenschist facies established by mineralogical indicators[26] and previous Raman-based estimates of regional peak metamorphic temperatures for the central part of the BGB[27] (Fig. 3, Supplementary Fig. 6, Supplementary Table 1). This confirms that the laminae are of syngenetic origin with the sandstone. Based on the combined evidence of carbonaceous composition, syngenicity, cohesiveness, sediment trapping behavior, and the presence of filamentous microstructures, the laminae are confidently identified as the fossilized remnants of microbial mats.

116 The presence of microbial mats on land during the Paleoarchean provides important insights
117 into the timing of certain evolutionary innovations required for terrestrialization. The Archean
118 land surface was likely a harsh environment subject to repeated desiccation, fluvial and/or
119 aeolian abrasion, and presumably, intense UV radiation. Its colonization suggests that the
120 terrestrial mats possessed a variety of adaptations, including tolerance to high shear stresses via
121 formation of cohesive and resistive mats, production of hygroscopic EPS (extracellular
122 polymeric substance) to maintain wetting during subaerial exposure, synthesis of UV-screening
123 pigments and an enhanced capacity for DNA-repair to cope with cellular damage induced by
124 desiccation and/or exposure to high-incidence UV radiation. It appears that terrestrial mats of
125 the Moodies Group already possessed such coping mechanisms at 3,220 Myr.
126
127 Our new report of terrestrial mat fossils adds to the known diversity of the Moodies ecosystem,
128 which includes large spheroidal microfossils[16], widespread shallow marine tufted microbial
129 mats with trapped gas bubbles[17–19], and remnants of cavity-dwelling microbes thriving beneath
130 the mats[20]. These coeval marine microbial communities are preserved in sandstones in the
131 nearby Saddleback Syncline that show clear bidirectional paleocurrent patterns characteristic
132 of deposition under tidal influence[19].
133
134 To better characterize and distinguish the paleobiological context of these unique terrestrial
135 mats from their marine counterparts, we subsampled mat-rich horizons from both and analyzed
136 them for the carbon isotope composition of organic matter and for bulk nitrogen isotope
137 composition. We also examined dolomite remnants that occur as bladed to blocky cement in
138 mm- to cm-sized bedding-parallel cavities beneath the mats[19,20] in both environments. In places
139 these carbonates are plastically deforming and rupture the mats, which further indicates their
140 early diagenetic formation, prior to sandstone lithification (Supplementary Fig. 7). All
141 carbonates yielded homogeneous mean $\delta^{13}C_{carb}$ values of +0.2 ±0.2‰ and $\delta^{18}O_{carb}$ values of -

15.4‰ ±0.2‰ (n=16, Supplementary Table 2), common values for dolomitic carbonates of Archean age that rule out significant secondary exchange between carbon pools after burial.

Carbon fixation in Moodies Group microbial mats

The carbon isotope composition of preserved organic matter provides a more direct link to metabolic activity during mat growth. In the terrestrial mats, $\delta^{13}C_{org}$ values range between -23.6‰ and -17.9‰, with a mean of -21.2‰ (n=36; Supplementary Table 3). These values contrast with isotopically lighter $\delta^{13}C_{org}$ values of microbial communities from the coeval marine deposits, ranging between -33.9‰ and -21.3‰, with a mean of -27.4 (n=30; Fig. 4). The observed difference between the two data sets is statistically significant (two-tailed Welsh's t-test, $p<0.0001$). The ~6‰ shift to heavier $\delta^{13}C_{org}$ values in the terrestrial realm thus suggests significant environmental and metabolic diversity across this Paleoarchean ecosystem landscape.

There are several non-mutually exclusive explanations for this shift. Firstly, cell size, growth rate, and species-specific differences in CO_2 diffusion rates all influence ε_p, the carbon isotopic fractionation factor associated with phototrophic carbon fixation[28,29]. However, the influence of these factors on ε_p tends toward zero[29] as pCO_2 approaches the elevated values inferred for the Archean[30], and some bacterial species exhibit little variation even at low CO_2 concentrations[31]. A more likely explanation for this shift is a mixing of carbon sources with different isotopic compositions. The terrestrial samples exhibit a narrow distribution in $\delta^{13}C_{org}$ values, suggesting a relatively homogenous source centered around -21‰. This $\delta^{13}C_{org}$ composition is consistent with autotrophic carbon fixation via the Calvin-Benson cycle[32,33], whether by oxygenic or anoxygenic phototrophs. Marine samples reach values that are isotopically as heavy, yet cover a larger spread extending to lighter $\delta^{13}C_{org}$ values, some as low

as -34‰. These features suggest that in the marine realm, mixing occurred between material with the same isotopic composition (-21‰) as terrestrial samples and material with carbon that was isotopically lighter than -34‰. Under high pCO_2, carbon fixed by the Calvin-Benson cycle is unlikely to reach such low values[34], which are best explained instead by biomass derived from other carbon fixation pathways, notably the reductive Acetyl Co-A (Wood–Ljungdahl) pathway[34–36]. This includes acetogenic bacteria, methanogens, and sulfate reducers that, with the exception of some examples of the latter[37], are obligate anaerobes. The terrestrial mat samples are rather remarkable in that the light carbon isotope signature that should be associated with alternative fixation pathways such as the reductive Acetyl Co-A pathway is not observed.

We suggest that this disparity reflects differences in fermentative or respiratory processes occurring in the mats along a paleoenvironmental transect. One possibility is that higher sedimentation rates in the terrestrial realm promoted rapid burial of carbon formed at the mat surface via the Calvin-Benson pathway, while lower sedimentation rates in marine settings permitted greater expression of the anaerobic reductive Acetyl-CoA pathway at depth in the mat. A related possibility is that distinct microbial communities inhabited these different environments. Indeed, in modern microbial mats, production of CH_4 is independent of diel cycling between ambient oxic and anoxic water conditions, yet appears strongly suppressed in intertidal mats and enhanced in subtidal mats as the result of differences in their anaerobic community structure at depth[38]. These include differences in the activity of sulphate reducers, who outcompete methanogens for organic substrates even at sulphate concentrations as low as 60 μM[39]. The local presence of sulphate in supratidal to braided-fluvial environments during Moodies Group deposition is indicated by common pseudomorphic relics of gypsum[40] and isotopic evidence for sulphate reduction in Moodies Group paleosols[14]. However, other possibilities exist that may have resulted in a greater contribution of carbon from pathways other than Calvin-Benson, such as the Wood-Ljungdahl pathway, in the marine realm. It has

been suggested that hydrogen gas was the principal electron donor for photosynthetic mat growth in the 3,416 Myr Buck Reef Chert (Onverwacht Group, also in the BGB)[3,41]. Anoxygenic phototrophs growing on hydrogen using the reverse tricarboxylic acid or 3-hydroxypropionate CO_2 fixation pathways are characterized by carbon isotope compositions that tend to be heavier than -14‰ (see review in ref. 36 and references therein), for which no evidence is observed in our dataset. However, if locally abundant, hydrogen might have been important in stimulating anaerobic metabolism via the Wood-Ljungdahl pathway. Both oxygenic and anoxygenic phototrophs may themselves produce significant quantities of hydrogen gas via bi-directional hydrogenases, and under conditions of nitrogen limitation, this may also occur via a nitrogenase-catalyzed side reaction[42]. In the terrestrial realm, rapid burial, the increased availability of sulphate and/or fixed nitrogen, and a depressed role for hydrogen, are all plausible explanations for the contrasting carbon pools preserved in the mats, however it is difficult to draw further inference based on carbon isotope data alone.

Isotopic insight into nitrogen cycling 3,220 Myr ago

Bulk nitrogen isotopic compositions of mat samples also record a significant contrast between the two paleoenvironments that points to differences in mat community structure and respiratory processes. $\delta^{15}N$ values of marine mats range between -0.7‰ and +3.1‰, with an average of +1.8‰ (n=10), in contrast to terrestrial $\delta^{15}N$ values that are generally more positive, ranging between +1.9‰ and +5.6‰ with a mean of +4.3‰ (n=10, Fig. 4, Supplementary Table 4). The $\delta^{15}N$ values of the two sample sets are statistically different, even if the two marine data points that are lowest in $\delta^{15}N$ are considered as outliers (two-tailed Welsh's t-test, $p<0.002$). While the marine samples show near-zero values consistent with atmospheric nitrogen fixation, values of up to +5‰ in the terrestrial samples are outside the range of typical fractionations associated with growth on atmospheric N_2. C/N ratios range from 8 to 60 and show no covariation with $\delta^{15}N$ values; similar to peak metamorphic temperatures determined by Raman

spectroscopy (Supplementary Table 1), C/N ratios show no significant differences between terrestrial and marine mat samples (Supplementary Figure 8), suggesting that the differences observed in $\delta^{15}N$ are not the expression of different diagenetic or metamorphic histories (e.g., ref. 34). Moreover, it has been shown that $\delta^{15}N$ values are resistant to modification during low grade metamorphism[43], in the case of kerogen varying no more than 1‰ for sediments reaching greenschist facies[44]. The lowest C/N ratios observed are probably linked to the presence of clay minerals that retain nitrogen produced during diagenesis. Total nitrogen contents (12–64 ppm, Supplementary Table 4) show no significant differences between marine and terrigenous sediments, and show no relation to clay content (~17 to 32% illite and muscovite in samples for which X-ray diffraction was performed), suggesting that variable contributions of nitrogen bound to clay, including allochthonous clay, cannot explain the isotopic contrast between the two datasets, which are instead most likely recording different primary compositions of mat biomass.

Three different biological mechanisms are known to produce biomass with $\delta^{15}N$ compositions greater than +2‰ (see ref. 45 for a detailed discussion). The first, and the only mechanism possible in the absence of oxidative nitrogen cycling, is partial assimilation of NH_4^+, whereby preferential uptake of $^{14}NH_4^+$ can drive the residual NH_4^+ toward isotopically heavier values (e.g., ref. 46). However, only after most of the NH_4^+ pool has been assimilated would residual NH_4^+ achieve values as heavy as +5‰ and we see no evidence in our dataset for light isotope enrichments that would indicate this process. The two remaining hypotheses are partial nitrification and/or partial denitrification, both of which require oxidative nitrogen cycling in the terrestrial mats. Partial nitrification requires a local source of O_2 (with or without Mn oxide intermediates) and has only been observed to generate such positive values in stratified water bodies where O_2 concentrations are highly dynamic as the result of seasonal overturning[45], which does not apply to the fluvial setting of the terrestrial mats. Finally, partial denitrification

of a stable nitrate pool is the process that is most commonly evoked for the generation of isotopically heavy $\delta^{15}N$ compositions in organic matter[43,45], and would also appear to be the most parsimonious explanation for the isotopically heavy $\delta^{15}N$ compositions of the terrestrial mats.

The source of nitrate to the terrestrial mat ecosystem may have been atmospheric. Prebiotic generation of fixed nitrogen (NO^-, NO_2^-, and NO_3^-) in the atmosphere by lightning discharge at $pO_2 < 10^{-5}$ present atmospheric level (PAL) is estimated to be around 2 to 4 x 10^{11} g N per year[47,48], which translates to a global surface flux of 0.1 to 0.2 μg N m^{-2} day^{-1}. While this flux may have been too diffuse to be a significant source of fixed nitrogen to the marine biosphere[49], fluvial mats would have had access to fixed nitrogen that is integrated over a larger area by surface runoff. We calculate the drainage area required to supply an atmospheric fixed nitrogen flux to mats at a rate that is comparable to that of nitrogen fixation by modern intertidal microbial mats (6 to 79 mg N m^{-2} day^{-1})[50] to be only 0.02 to 0.62 km^2. In other words, rainout of fixed nitrogen onto the early land surface should have had a profound influence on nitrogen cycling in early terrestrial ecosystems, one that appears expressed in the contrasting nitrogen isotope compositions of microbial mat biomass between terrestrial and marine settings in the Moodies Group.

Our observations rejoin those from the slightly younger (~3,000 Myr) Mesoarchean fluvio-lacustrine Lalla Rookh sandstone (W. Australia) where a contrast in the carbon isotope composition of organic matter has also been observed[34], albeit relative to marine sediments of similar age from other localities, whereas our comparison is made on approximately coeval sediments from the same basin. In the Lalla Rookh sandstone, the carbon isotopic contrast occurred in the reverse sense (with more important $\delta^{13}C$ depletion in lacustrine sediments) and

without any evidence for oxidative nitrogen cycling. Nonetheless, the ensemble of emerging evidence indicates that microbial communities already inhabited terrestrial surface environments, and fundamentally differed from their marine counterparts in their biogeochemical cycling of carbon and nitrogen, at the dawn of continental emergence ca. 3,220 Myr ago.

References

1. Nutman, A. P., Bennett, V. C., Friend, C. R. L., Van Kranendonk, M. J. & Chivas, A. R. Rapid emergence of life shown by discovery of 3,700-million-year-old microbial structures. *Nature* **537,** 535–538 (2016).
2. Allwood, A. C., Walter, M. R., Kamber, B. S., Marshall, C. P. & Burch, I. W. Stromatolite reef from the Early Archaean era of Australia. *Nature* **441,** 714–718 (2006).
3. Tice, M. M. & Lowe, D. R. Photosynthetic microbial mats in the 3 , 416-Myr-old ocean. *Nature* **431,** 549–552 (2004).
4. Wacey, D., Kilburn, M. R., Saunders, M., Cliff, J. & Brasier, M. D. Microfossils of sulphur-metabolizing cells in 3.4-billion-year-old rocks of Western Australia. *Nat. Geosci.* **4,** 698–702 (2011).
5. Dodd, M. S. *et al.* Evidence for early life in Earth's oldest hydrothermal vent precipitates. *Nature* **543,** 60–64 (2017).
6. Flament, N., Coltice, N. & Rey, P. F. The evolution of the $^{87}Sr/^{86}Sr$ of marine carbonates does not constrain continental growth. *Precambrian Res.* **229,** 177–188 (2013).
7. The term "terrestrial" has multiple definitions; here we follow convention from literature on the Precambrian biosphere by considering any life on the emerged continental surface, aquatic or subaerial, as terrestrial (see supplementary text).
8. Beraldi-Campesi, H. Early life on land and the first terrestrial ecosystems. *Ecol. Process.* **2,** 1 (2013).
9. Wellman, C. H. & Strother, P. K. The terrestrial biota prior to the origin of land plants (embryophytes): a review of the evidence. *Palaeontology* **58,** 601–627 (2015).
10. Watanabe, Y., Martini, J. E. & Ohmoto, H. Geochemical evidence for terrestrial ecosystems 2.6 billion years ago. *Nature* **408,** 574–578 (2000).
11. Rye, R. & Holland, H. D. Life associated with a 2.76 Ga ephemeral pond?: Evidence from Mount Roe #2 paleosol. *Geology* **28,** 483–486 (2000).
12. Crowe, S. A. *et al.* Atmospheric oxygenation three billion years ago. *Nature* **501,** 535–8 (2013).
13. Mukhopadhyay, J. *et al.* Oxygenation of the Archean atmosphere: New paleosol constraints from eastern India. *Geology* **42,** 923–926 (2014).
14. Nabhan, S., Wiedenbeck, M., Milke, R. & Heubeck, C. Biogenic overgrowth on detrital pyrite in ca. 3.2 Ga Archean paleosols. *Geology* **44,** 763–766 (2016).
15. Djokic, T., Van Kranendonk, M. J., Campbell, K. A., Walter, M. R. & Ward, C. R. Earliest signs of life on land preserved in ca. 3.5 Ga hot spring deposits. *Nat. Commun.* **8,** 1–8 (2017).
16. Javaux, E. J., Marshall, C. P. & Bekker, A. Organic-walled microfossils in 3.2-billion-year-old shallow-marine siliciclastic deposits. *Nature* **463,** 934–8 (2010).
17. Noffke, N., Eriksson, K. A., Hazen, R. M. & Simpson, E. L. A new window into Early Archean life: Microbial mats in Earth's oldest siliciclastic tidal deposits (3.2 Ga Moodies Group, South Africa). *Geology* **34,** 253 (2006).
18. Heubeck, C. An early ecosystem of Archean tidal microbial mats (Moodies Group, South Africa, ca. 3.2 Ga). *Geology* **37,** 931–934 (2009).
19. Homann, M., Heubeck, C., Airo, A. & Tice, M. M. Morphological adaptations of 3.22 Ga-old tufted microbial mats to Archean coastal habitats (Moodies Group, Barberton Greenstone Belt, South Africa). *Precambrian Res.* **266,** 47–64 (2015).
20. Homann, M. *et al.* Evidence for cavity-dwelling microbial life in 3.22 Ga tidal deposits. *Geology* **44,** 51–54 (2016).
21. Eriksson, K. A., Simpson, E. L. & Mueller, W. U. An unusual fluvial to tidal transition

in the mesoarchean Moodies Group, South Africa: A response to high tidal range and active tectonics. *Sediment. Geol.* **190,** 13–24 (2006).
22. Heubeck, C. *et al.* Geological constraints on Archean (3.22 Ga) coastal-zone processes from the Dycedale Syncline, Barberton Greenstone Belt. *South African J. Geol.* **119,** 495–518 (2016).
23. De Ronde, C. E. J. & Kamo, S. L. An Archaean arc-arc collisional event: A short-lived (ca 3 Myr) episode, Weltevreden area, Barberton greenstone belt, South Africa. *J. African Earth Sci.* **30,** 219–248 (2000).
24. Heubeck, C. *et al.* Timing of deposition and deformation of the Moodies Group (Barberton Greenstone Belt, South Africa): Very-high-resolution of Archaean surface processes. *Precambrian Res.* **231,** 236–262 (2013).
25. Farber, K., Dziggel, A., Trumbull, R. B., Meyer, F. M. & Wiedenbeck, M. Tourmaline B-isotopes as tracers of fluid sources in silicified Palaeoarchaean oceanic crust of the Mendon Formation, Barberton greenstone belt, South Africa. *Chem. Geol.* **417,** 134–147 (2015).
26. Xie, X., Byerly, G. R. & Ferrell Jr., R. E. IIb trioctahedral chlorite from the Barberton greenstone belt: crystal structure and rock composition constraints with implications to geothermometry. *Contrib. to Mineral. Petrol.* **126,** 275–291 (1997).
27. Tice, M. M., Bostick, B. C. & Lowe, D. R. Thermal history of the 3.5–3.2 Ga Onverwacht and Fig Tree Groups, Barberton greenstone belt, South Africa, inferred by Raman microspectroscopy of carbonaceous material. *Geology* **32,** 37 (2004).
28. Popp, B. N. *et al.* Effect of Phytoplankton Cell Geometry on Carbon Isotopic Fractionation. *Geochim. Cosmochim. Acta* **62,** 69–77 (1998).
29. Hayes, J. M., Strauss, H. & Kaufman, A. J. The abundance of in marine organic matter and isotopic fractionation in the global biogeochemical cycle of carbon during the past 800 Ma. *Chem. Geol.* **161,** 103–125 (1999).
30. Driese, S. G. *et al.* Neoarchean paleoweathering of tonalite and metabasalt: Implications for reconstructions of 2.69Ga early terrestrial ecosystems and paleoatmospheric chemistry. *Precambrian Res.* **189,** 1–17 (2011).
31. Laws, E. A., Popp, B. N., Cassas, N. & Tanimoto, J. ^{13}C discrimination patterns in oceanic phytoplankton: likely influence of CO_2 concentrating mechanisms, and implications for palaeoreconstructions. *Funct. plant Biol.* **29,** 323–333 (2002).
32. Schidlowski, M. A 3,800-million-year isotopic record of life from carbon in sedimentary rocks. *Nature* **333,** 313–318 (1988).
33. Eigenbrode, J. L. & Freeman, K. H. Late Archean rise of aerobic microbial ecosystems. *Proc. Natl. Acad. Sci.* **103,** 15759–15764 (2006).
34. Stüeken, E. E. & Buick, R. Environmental control on microbial diversification and methane production in the Mesoarchean. *Precambrian Res.* **304,** 64–72 (2018).
35. Slotznick, S. P. & Fischer, W. W. Examining Archean methanotrophy. *Earth Planet. Sci. Lett.* **441,** 52–59 (2016).
36. Havig, J. R., Hamilton, T. L., Bachan, A. & Kump, L. R. Sulfur and carbon isotopic evidence for metabolic pathway evolution and a four-stepped Earth system progression across the Archean and Paleoproterozoic. *Earth-Science Rev.* **174,** 1–21 (2017).
37. Baumgartner, L. K. *et al.* Sulfate reducing bacteria in microbial mats: Changing paradigms, new discoveries. *Sediment. Geol.* **185,** 131–145 (2006).
38. Hoehler, T. M., Bebout, B. M. & Des Marais, D. J. The role of microbial mats in the production of reduced gases on the early Earth. *Nature* **412,** 324–327 (2001).
39. Lovley, D. R. & Klug, M. J. Sulfate reducers can outcompete methanogens at freshwater sulfate concentrations. *Appl. Environ. Microbiol.* **45,** 187–92 (1983).
40. Nabhan, S., Luber, T., Scheffler, F. & Heubeck, C. Climatic and geochemical implications of Archean pedogenic gypsum in the Moodies Group (~3.2Ga), Barberton

Greenstone Belt, South Africa. *Precambrian Res.* **275,** 119–134 (2016).
41. Tice, M. M. & Lowe, D. R. Hydrogen-based carbon fixation in the earliest known photosynthetic organisms. *Geology* **34,** 37 (2006).
42. Bandyopadhyay, A., Stöckel, J., Min, H., Sherman, L. A. & Pakrasi, H. B. High rates of photobiological H2 production by a cyanobacterium under aerobic conditions. *Nat. Commun.* **1,** 139 (2010).
43. Ader, M. *et al.* Interpretation of the nitrogen isotopic composition of Precambrian sedimentary rocks: Assumptions and perspectives. *Chem. Geol.* **429,** 93–110 (2016).
44. Ader, M. *et al.* Nitrogen isotopic evolution of carbonaceous matter during metamorphism: Methodology and preliminary results. *Chem. Geol.* **232,** 152–169 (2006).
45. Stüeken, E. E. A test of the nitrogen-limitation hypothesis for retarded eukaryote radiation: Nitrogen isotopes across a Mesoproterozoic basinal profile. *Geochim. Cosmochim. Acta* **120,** 121–139 (2013).
46. Papineau, D. *et al.* High primary productivity and nitrogen cycling after the Paleoproterozoic phosphogenic event in the Aravalli Supergroup, India. *Precambrian Res.* **171,** 37–56 (2009).
47. Kasting, J. F. & Walker, J. C. G. Limits on oxygen concentration in the prebiological atmosphere and the rate of abiotic fixation of nitrogen. *J. Geophys. Res.* **86,** 1147 (1981).
48. Navarro-gonz, R., Molina, M. J. & Molina, L. T. Nitrogen fixation by volcanic lightning in the early Earth. *Geophys. Res. Lett.* **25,** 3123–3126 (1998).
49. Stüeken, E. E., Kipp, M. A., Koehler, M. C. & Buick, R. The evolution of Earth's biogeochemical nitrogen cycle. *Earth-Science Rev.* **160,** 220–239 (2016).
50. Joye, S. B. & Paerl, H. W. Nitrogen Cycling In Microbial Mats - Rates And Patterns Of Denitrification And Nitrogen-Fixation. *Mar. Biol.* **119,** 285–295 (1994).

Corresponding author

Correspondence and request for materials should be addressed to M.H.

(martin.homann@univ-brest.fr)

Acknowledgements

This work was supported by Deutsche Forschungsgemeinschaft (DFG) grant He2418/13–1, LabexMER ANR-10-LABX-19, and Prestige COFUND-GA-2013-609102. We thank N. and D. Oosthuizen for access to the private Mountainlands nature reserve, S. Bläsing and M. Grund for assistance with sample collection, J.-P. Oldra for thin section preparation, and O. Lebeau, C. Tanvet, C. Liorzou, M.-L. Rouget, and B. Gueguen for assistance with isotopic and elemental analysis.

Author contributions

M.H. and C.H. carried out field work and collected samples in South Africa. P.S., M.A., and S.V.L. helped with the acquisition and interpretation of elemental and isotopic data. M.V.Z. and J.G. performed Raman analysis. B.K., I.S.F., A.A. and M.J.V.K. contributed to the discussion of the data. M.H. wrote the manuscript with significant contributions from all co-authors.

Figures

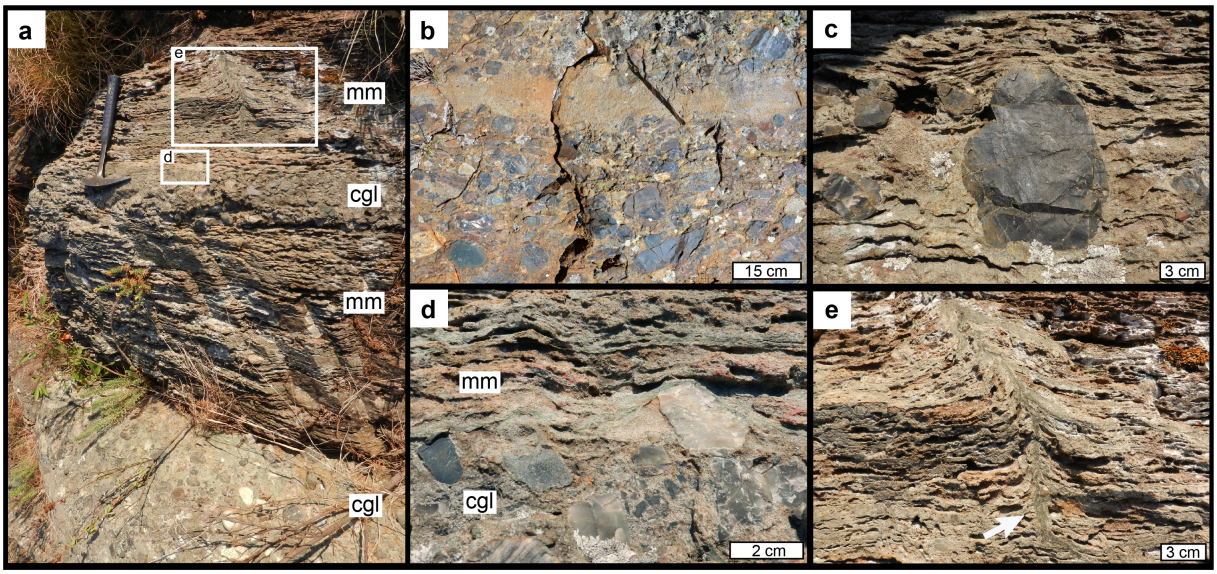

Figure 1. Field photographs of fluvial sandstones and conglomerates hosting fossil terrestrial mats from the 3,220 Myr old Moodies Group. a, Overview photograph showing interbedded fossil microbial mats (mm) and conglomerates (cgl). **b**, Mat-associated fluvial conglomerate, composed of subrounded pebbles and cobbles. **c, d**, Microbial mats draping and onlapping interbedded clasts within the sandstones and on top of conglomerate beds (close-up view of the framed area in (a). **e**, Fluid-escape structure with well-defined central channel (arrow) that vertically disrupts the densely mat-laminated sandstone (close-up view of the framed area in (a).

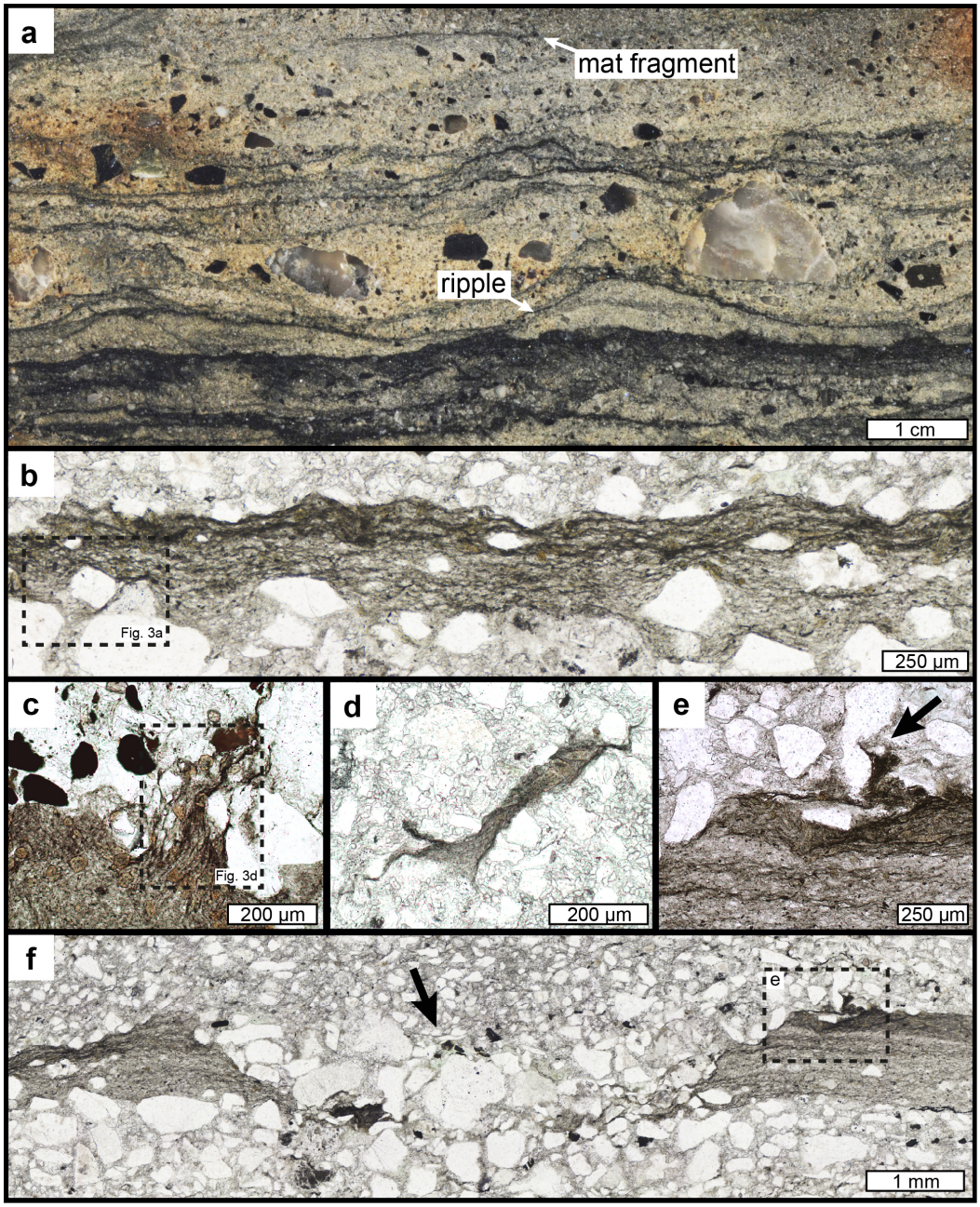

Figure 2. Reflected and transmitted light photomicrographs of the terrestrial microbial mats of the Moodies Group. a, Dark carbonaceous laminae of the fossil mats draping horizontally laminated and rippled sand and onlapping pebbles. Chips of eroded mat fragments are preserved in cross-laminated, granular sandstone. **b,** Dense meshwork of interwoven filamentous microstructures with trapped detrital grains. **c**, Bundled filamentous structures in upper part of the mat. **d**, Close-up view of eroded mat fragment. **e,** Partially eroded microbial mat laminae due to abrasion by impacting sand grains (arrow) and **f,** Erosional truncation of the mat by small channel (arrow).

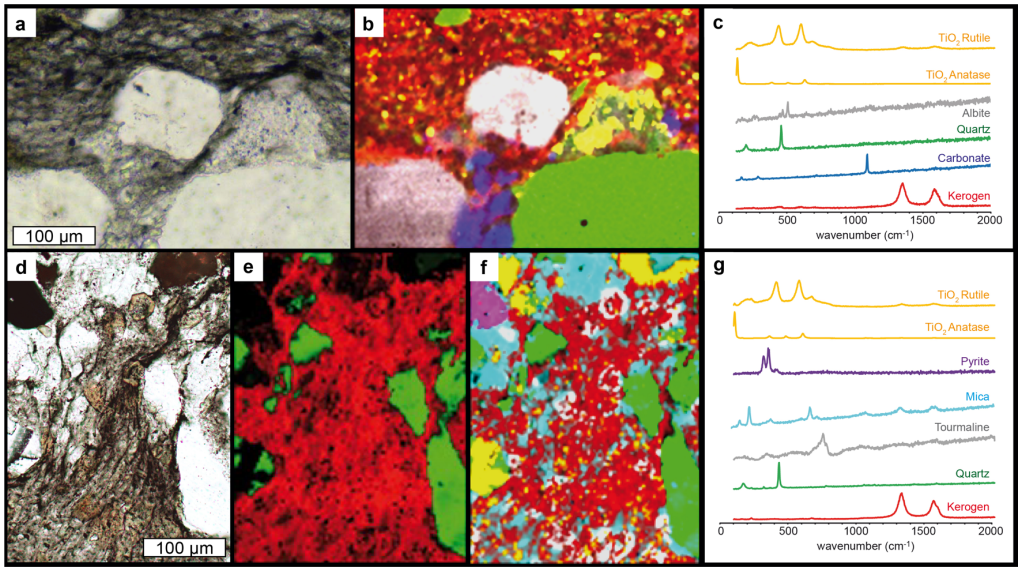

Figure 3. Transmitted light photomicrographs of preserved kerogenous laminae (a) and filamentous microstructures (d) of the terrestrial mats, with corresponding Raman component maps for mineral phases and G-peak intensity for kerogenous phases (**b, e, f**), and representative Raman component spectra (**c, g**). Note that the analyzed areas are close-up views of the samples shown in Figure 2B and 2C, respectively.

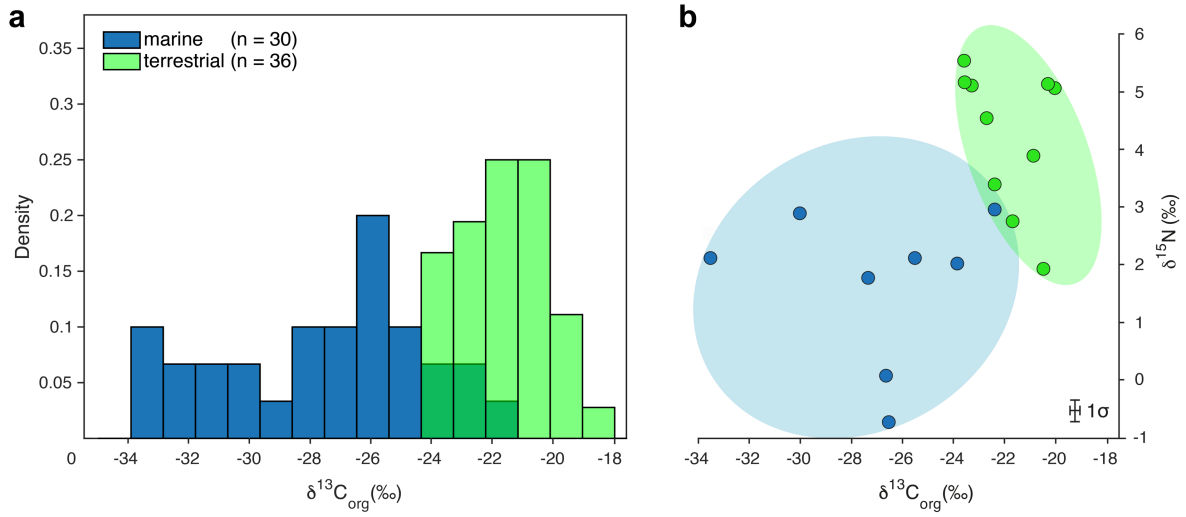

Figure 4. Carbon isotope composition of organic matter and bulk nitrogen isotope composition from terrestrial (green) and marine (blue) microbial mats of the Paleoarchean Moodies Group. a, Histogram of organic carbon $\delta^{13}C_{org}$ and **b,** $\delta^{13}C_{org}$ versus $\delta^{15}N$ values for both environments.

Methods

Optical microscopy. Standard 30-µm-thick, polished thin sections, oriented perpendicular to bedding, were analyzed using an Olympus BX60 petrographic microscope and a Zeiss Axio Scope.A1 equipped with a 63x oil objective lens. High resolution scans of entire thin sections were performed with a Zeiss Axio Zoom v16 motorized stereo microscope at the IPGP, Paris.

Raman spectroscopy. Raman analyses were performed using a Renishaw InVia Raman microscope coupled to an Olympus BX61 Confocal microscope, within the PARI analytical platform at the IPGP in Paris. Measurements were made with a 514 nm-excitation (Ar-ion laser) and adjusted to an on-sample intensity of 0.2 mW with a spot size of < 2 µm (50x objective). Beam centering and Raman spectral calibration were performed on a pure silicon chip with a specific Raman band at 520.4 cm^{-1}. All spectra were detected using 1800 l/mm grating, and a detector configuration in streamspot mode, providing a spectral range of 2000 cm^{-1} in static mode. Individual spot analyses were obtained in both static mode (2 x 20 s exposure, centered at 1150 cm^{-1} with a spectral range of 100-2000 cm^{-1}) and extended mode (1 x 20 s exposure, spectral range 100-4000 cm^{-1}). In order to determine Raman spectral indicators of the carbonaceous fractions, the individual spectra were truncated to 900-1900 cm^{-1}, and a linear background subtraction was performed, using the program Wire 2.0. Peak-decomposition was performed using two generally reported methods: a) a 2-peak fit, assigning a D-peak at ca. 1350 cm^{-1} and a G-peak at ca. 1600 cm^{-1} (following the procedure outlined in Sforna et al.[51]), b) a 4-peak fit, assigning a D1-, D2-, D3-, and G-peak at ca. 1350 cm^{-1}, 1620 cm^{-1}, 1500 cm^{-1}, and 1600 cm^{-1}, respectively (following the procedure outlined in Sforna et al.[51], Supplementary Fig. 6). In all obtained spectra a D4-peak at ca. 1200 cm^{-1} was absent and was therefore not assigned during the peak decomposition procedure. Spectral data of the decomposed peaks (position, width, height, area) were recorded and used for calculating the Raman indicators D-FWHM (D-peak full width at half maximum) and ID/IG (height-based D/G) using the 2-peak fit, and D1-

FWHM, R1 (height-based D1/G) and R2 (area-based D1/D1+D2+G) using the 4-peak fit. Two geothermometers could then be calculated, that of Beyssac et al.[52] using T= -445xR2 + 641, and that of Kouketsu et al.[53] using T= (-2.15 x D1-FWHM) + 478 (see Supplementary Table 1). Raman hyperspectral maps were obtained for selected areas within the thin sections 14-452-1B2 and 14-452-1B9, in streamspot mode (point-by-point scanning) using 1 x 6 s or 1 x 10 s exposures per point. Raman maps were generated using the software Wire 2.0 by selecting representative spectra for each component (minerals and kerogen) within the hyperspectral dataset (Fig. 3) and subsequent component analysis for each spectral point was determined using a background subtraction with a 2nd order polynomial fit. Maps of individual components were subsequently merged using the imaging program ImageJ.

Carbon isotope analysis. For isotope analysis of organic carbon, large rock samples (up to 50x20 centimeters) were collected in the field from the freshest and least weathered outcrops available. In the lab all outer surfaces of the rocks where removed with a rock saw and were cut into smaller blocks, devoid of any cracks or fractures. Afterwards, mat horizons, 2 – 10 mm thick, were cut out individually with a thin rock saw and broken into smaller pieces, cleaned in an ultrasonic bath and dried. The resultant material was then crushed into a fine powder using an automated agate mill grinder, which was cleaned with pure quartz sand, distilled water, and ethanol between each run. The powders were decarbonated with 6N HCl for 12 hours then warmed at 80°C for 2h in a fume hood. Residues were rinsed with Milli-Q water, then centrifuged three to four times until they approached a neutral pH. 10 to 50 mg of decarbonated samples were loaded into tin capsule and analyzed for their carbon isotopic composition at the Pôle Spectométrie Océan (PSO, Brest, France) using a Thermo Scientific Delta V plus mass spectrometer coupled to a Flash 2000 elemental analyzer. Isotopic results are reported in delta notation against the V-PDB standard (Vienna Pee Dee Belemnite) with an average analytical error of 0.12‰ (2σ, Supplementary Table 3). For C and O isotope composition of the mat-

associated carbonates, CO_2 was released from powdered samples by reaction with 100% H_3PO_4 at 72ºC in a Kiel IV automated carbonate preparation device. The CO_2 was analyzed using for isotope compositions using a Finnigan MAT 253 mass spectrometer. $^{18}O/^{16}O$ and $^{13}C/^{12}C$ ratios were also expressed in delta notation relative to the V-PDB standard (Supplementary Table 2). Precision for $\delta^{18}O$ and $\delta^{13}C_{carb}$ was 0.2‰ (2σ) and 0.1‰ (2σ), respectively.

Nitrogen isotope analysis. Individual carbonaceous mat laminae were manually separated from fresh and unweathered sandstone samples (as described above), ground in an automated agate mill grinder, and sieved to ensure a grain size smaller than 140 µm. Bulk rock $\delta^{15}N$ measurements were performed as they have been suggested to be more likely to record the primary isotopic composition of the original biomass in kerogen-poor greenschist-facies metasediments as compared to measurements of kerogen isolates[54]. To concentrate nitrogen in the insoluble residue, the samples were first decarbonated in HCl 6N for 12h overnight at room temperature, followed by 2h at 80°C in a fume hood. Residual material was rinsed three times with Milli-Q water, then centrifuged and dried at 50°C overnight. Approximately 500-1400 mg of powdered samples were analyzed following the method detailed in Ader et al.[55]. Conventional sealed tube combustion with CuO_2 and Cu rods (but in this study without CaO grains) was used to convert total nitrogen to N_2 (Dumas combustion), which was then purified using a secondary vacuum extraction line as shown in Figure 1 of Li et al.[56] N_2 nitrogen isotope ratio measurements were performed using a dual inlet Thermo-Fisher Delta V+ mass spectrometer at the IPGP in Paris (Supplementary Table 4). Each purified nitrogen gas sample was analyzed twice. Nitrogen blanks were lower than 0.1 micromoles, thus representing less than 10% of the measured nitrogen. External reproducibility of the $\delta^{15}N_{sed}$ measurements was ± 0.4 ‰ (1σ).

Data availability. The authors declare that all data supporting the study are available within the article and its Supplementary Information file.

References

51. Sforna, M. C., van Zuilen, M. A. & Philippot, P. Structural characterization by Raman hyperspectral mapping of organic carbon in the 3.46 billion-year-old Apex chert, Western Australia. *Geochim. Cosmochim. Acta* **124,** 18–33 (2014).
52. Beyssac, O., Goffé, B., Chopin, C. & Rouzaud, J. N. Raman spectra of carbonaceous material in metasediments: a new geothermometer. *J. Metamorph. Geol.* **20,** 859–871 (2002).
53. Kouketsu, Y. *et al.* A new approach to develop the Raman carbonaceous material geothermometer for low-grade metamorphism using peak width. *Isl. Arc* **23,** 33–50 (2014).
54. Stüeken, E. E., Zaloumis, J., Meixnerová, J. & Buick, R. Differential metamorphic effects on nitrogen isotopes in kerogen extracts and bulk rocks. *Geochim. Cosmochim. Acta* **217,** 80–94 (2017).
55. Ader, M., Boudou, J.-P., Javoy, M., Goffe, B. & Daniels, E. Isotope study on organic nitrogen of Westphalian anthracites from the Western Middle field of Pennsylvania (U.S.A.) and from the Bramsche Massif (Germany). *Org. Geochem.* **29,** 315–323 (1998).
56. Li, L., Cartigny, P. & Ader, M. Kinetic nitrogen isotope fractionation associated with thermal decomposition of NH3: Experimental results and potential applications to trace the origin of N2 in natural gas and hydrothermal systems. *Geochim. Cosmochim. Acta* **73,** 6282–6297 (2009).